Applied Physics B (2019) 125:4
https://doi.org/10.1007/s00340-018-7113-8

Applied Physics B
Lasers and Optics

Development of a few TW Ti:Sa laser system at 100 Hz for proton acceleration

Roberto Lera[1] · Pablo Bellido[2] · Isabel Sanchez[1] · Paula Mur[2] · Michael Seimetz[2] · Jose Maria Benlloch[2] · Luis Roso[3] · Alexandro Ruiz-de-la-Cruz[1]

Received: 20 June 2018 / Accepted: 27 November 2018 / Published online: 3 December 2018

Abstract
We report the development of a table-top high peak power Titanium:Sapphire (Ti:Sa) CPA laser working at 100 Hz capable of delivering 205 mJ, 55 fs pulses. Every amplification stage is pumped by Nd-doped solid-state lasers and fully powered by diodes. Thermal effects in the Ti:Sa amplifiers are compensated passively with optics. This system is intended to be used for proton acceleration experiments at high repetition rates.

1 Introduction

The field of laser-driven high intensity physics has grown steeply in the last years. Fields such as particle generation and acceleration show promising perspectives for the practical use of lasers: coherent X-ray generation [1], electron acceleration [2] and ion acceleration [3, 4]. For ion acceleration, the most common targetry are solid thin films of a metal or a plastic. Although the acceleration gradient is many orders of magnitude higher than that of a typical accelerator [5], the state-of-the-art laser-based accelerators do not provide enough current to be able to replace conventional radiofrequency technology. Furthermore, most of the experiments have been single shot and only a few have been multishot (10 Hz or higher repetition rate) [6]. This is due to the lack of both higher repetition rate targetry and lasers, hence the need for advances in the development of higher average power and high intensity lasers.

The introduction of the chirped pulse amplification (CPA) technique [7] fueled the development of high power, table-top ultrafast laser systems, such as Titanium:Sapphire (Ti:Sa) lasers, characterized by their broad bandwidth, able to support pulses as short as a few femtoseconds. However, its absorption band is located in a region of the visible spectrum where there are few available high energy laser sources. These are generally frequency doubled flash-lamp pumped Nd:YAG lasers; these types of laser can typically provide several joules of energy in tens of nanoseconds but their repetition rate rarely exceeds 10 Hz. Even though the peak power of a current Ti:Sa laser system can reach PW levels, the repetition rate of even TW-class CPA lasers remains limited to 10 Hz or less due to the lack of suitable high average power pump lasers. That is why the development of high power laser diodes at wavelengths able to pump Nd-doped crystals can improve the repetition rate of these pump lasers and therefore that of a pulsed Ti:Sa laser. However, the power output of the laser diodes is low compared to that of a flash-lamp, and a different architecture of diode-pumped solid-state lasers has to be employed to pump the Ti:Sa laser.

In this work, we present a compact Ti:Sa laser with peak power exceeding the TW level, 100 Hz repetition rate and pumped by diode-powered solid state lasers. The whole setup including all pump lasers fits into two optical tables, or an area of 7.35 m^2; it is based on CPA amplification and is composed of an oscillator, stretcher, a regenerative amplifier followed by two multipass amplifiers and a compressor as shown in Fig. 1. This system is intended to be used for laser-plasma particle acceleration so it includes a separate vacuum chamber where the compressor is located and another chamber where the experimental interaction of the laser with the target is performed.

✉ Roberto Lera
roberlm@usal.es

[1] Proton Laser Applications S.L, Av. Vilafranca del Penedés 11A, 08734 Olèrdola, Barcelona, Spain

[2] Instituto de Instrumentación para Imagen Molecular (I3M), CSIC-Universitat Politècnica de València, Camino de Vera S/N, 46022 Valencia, Spain

[3] Centro de Láseres Pulsados (CLPU), Parque Científico, Calle del Adaja 8, 37185 Villamayor, Salamanca, Spain

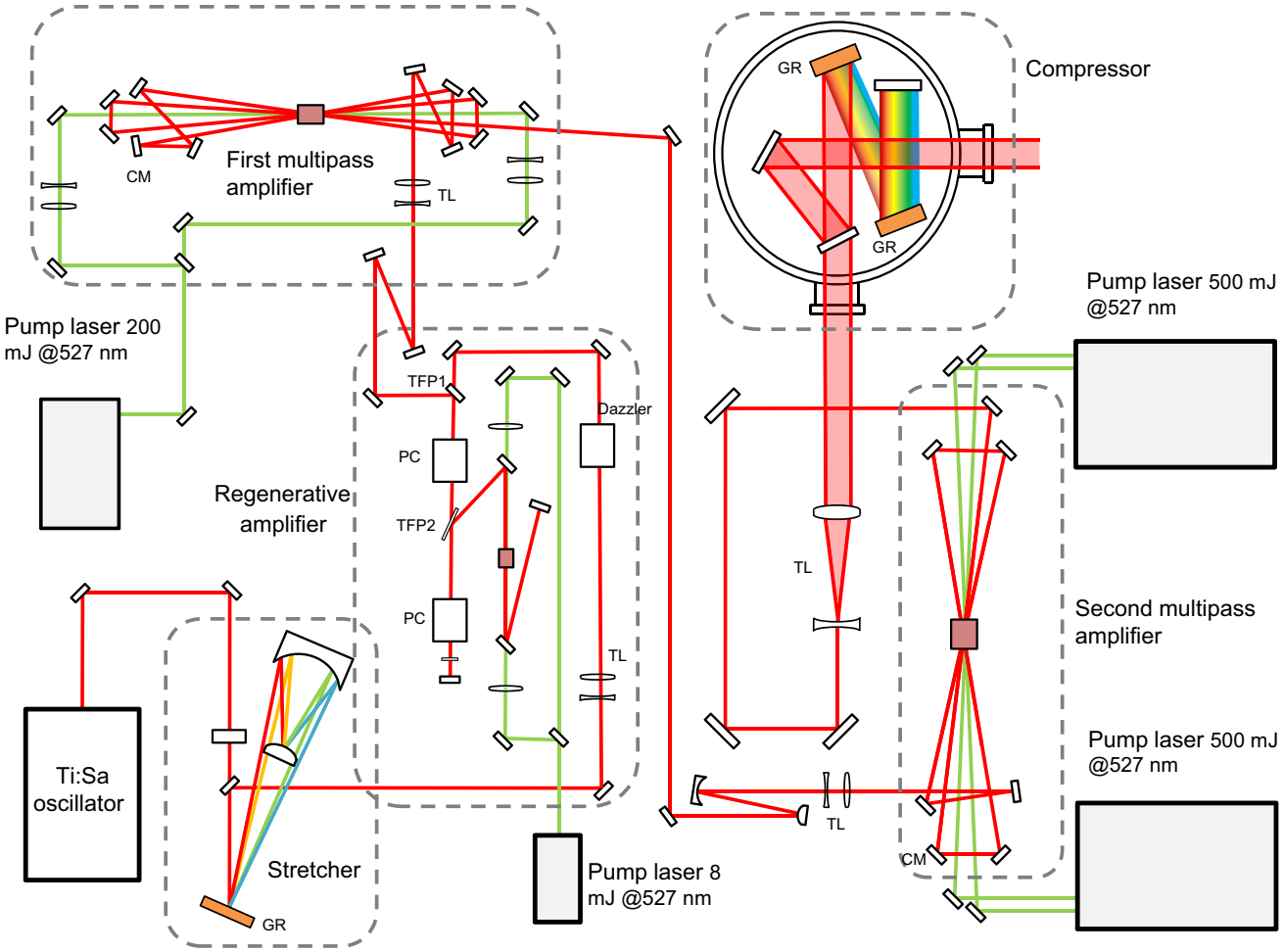

Fig. 1 Scheme of the CPA Ti:Sa laser. A pulse oscillator sends a beam of a few femtoseconds that is stretched in time in a pulse stretcher. Then it enters a chain of amplification that starts with a regenerative amplifier that is followed by a first multipass amplifier and ends with a second multipass amplifier. The CPA chain ends with a compressor installed in a vacuum chamber. *GR* grating, *PC* pockels cells, *TL* Galilean telescope, *CM* convex mirror, *TFP1&2* thin film polarizer

2 Laser system description

The schematic of the ultrashort laser is presented in Fig. 1. The femtosecond laser pulses are generated in a Kerr-lens mode locked Ti:Sa oscillator (Venteon). The 12 fs, 5 nJ seed pulses are stretched to 100 ps in an on-axis Öffner stretcher [8]. This stretcher consists of two metallic spherical mirrors, a 250-mm radius of curvature convex mirror and a 500-mm radius of curvature concave mirror; the diffraction grating (Horiba Jobin-Yvon) has 1200 grooves/mm and is placed 170 mm from the common center of curvature of the two mirrors. A pulse-shaping device (Dazzler from Fastlite [9]) is placed after the stretcher to control actively the spectral phase of the laser and act as a pulse picker.

Once stretched, the pulses selected by the Dazzler enter a regenerative amplifier pumped by 7 mJ, 100 ns pulses from the output of a Nd:YLF laser working at 100 Hz. The configuration of this amplifier is a z-folded cavity, containing a plane-parallel Ti:Sa crystal which measures $4 \times 6 \times 15$ mm and is anti-reflection coated. Two-fused silica Brewster windows, one on each side were added to minimize depolarization on each round trip. There are two pockels cells in the regenerative amplifier; the first one is located between two orthogonal thin film polarizers (TFP1 and TFP2 on Fig. 1) so that when it is powered pulses can enter the resonator through the second polarizer, rejecting all other pulses when off, effectively acting as a pulse picker. The second pockels cell traps the pulse inside the resonator and releases it when the maximum gain is achieved. The amplified pulse is then reflected at the TFP1 and continues its way towards the next amplification stage.

Before the next amplifier, a Faraday isolator is included to prevent feedback to the regenerative amplifier from the next amplification stages. The first multipass amplifier is

pumped by 200 mJ at 100 Hz from a Nd:YLF laser. The Ti:Sa crystal is plane-parallel, cylindrical 6 mm in diameter, 15 mm length, absorbs 92% of pump light and is placed on a water-cooled copper mount. This amplifier is constructed in a multipass bow–tie configuration where the seed beam undergoes up to four passes through the gain medium.

The output of the first multipass amplifier is magnified to a 8-mm diameter beam to be injected into the second multipass stage. This amplifier incorporates a $15 \times 16 \times 20$ mm crystal that is pumped by a total 1000 mJ of 527 nm radiation divided in four beams (two on each side) coming from two identical Nd:YLF lasers. The seed beam experiences three passes through the gain medium in this amplifier.

The pulse is finally compressed in a Treacy-type compressor made up of two diffraction gratings of identical characteristics to the one in the stretcher and enclosed in vacuum chamber.

3 Pump lasers

The increasing availability of high power laser diodes has driven the development of high average power solid-state lasers, particularly Nd-doped based [10–12]. However, the scarcity of high repetition rate lasers suitable for pumping a Ti:Sa laser compelled us develop our own pump lasers using a Nd-doped active medium powered by laser diodes. In collaboration with Monocrom S.L (Barcelona, Spain), we designed and constructed a pumping head comprised by a solid state cylindrical laser rod surrounded by cooling water and six stacks each containing six laser diodes of 150 W maximum optical output [13].

To create a laser capable of generating energetic pulses at high repetition rate, these pumping heads were used as the building blocks of a master oscillator power amplifier (MOPA) laser. The scheme of the laser is shown in Fig. 2. It consists of an oscillator with a single pumping head and two pairs of amplifiers for a total of five pumping heads. To improve the overall efficiency of the laser, the scheme of the laser included a second harmonic generation (SHG) stage between both pairs of amplifiers so that the seed from the oscillator is amplified in the first pair of amplifiers and after going through the SHG crystal, the unconverted fundamental harmonic of the laser is further amplified by the second pair of amplifiers instead of being dumped. After the second pair of amplifiers, there is another SHG stage. This design improves the overall efficiency of the laser and lowers its cost and complexity.

Nd:YLF was chosen as the active medium, as it has some advantages with respect to Nd:YAG, including higher stored energy and less thermal lensing optical power. For a MOPA, these properties mean more gain in the amplifiers and less restrictions due to thermal management. The wavelength of the laser was chosen as the 1053 nm line of Nd:YLF.

The oscillator of this laser is powered by one pumping head loaded with a 5-mm diameter, 0.8% at doping

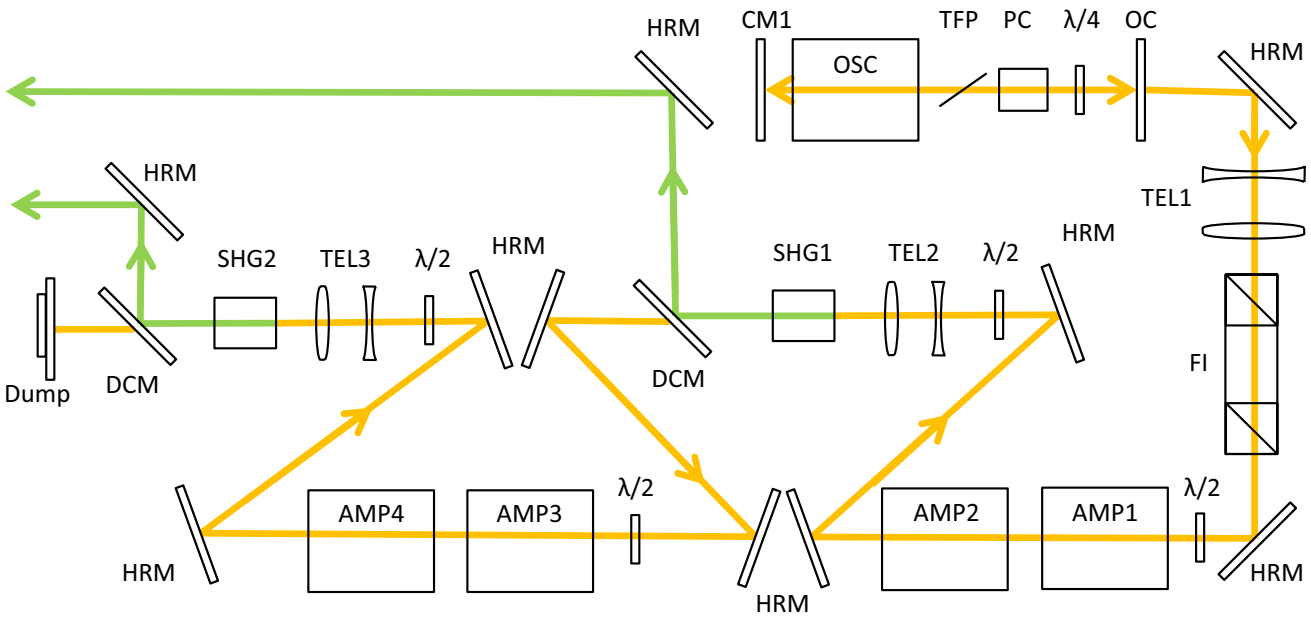

Fig. 2 Scheme of a MOPA Nd:YLF laser with five pumping heads (OSC, AMP1-4). CM1 and OC are the two mirrors that comprise the oscillator, along with a pumping heads, a thin film polarizer (TFP), a pockels cell (PC) and a quarter waveplate $\lambda/4$. The setup includes a Faraday isolator (FI) and three telescopes (TEL1-3). (SHG1&2) represent non-linear crystals for second harmonic conversion. There are two dichroic mirrors (DCM1&2) and a beam dump. HRM are high reflectivity mirrors

c-cut Nd:YLF rod. The resonator length was 55 cm and comprised a 3000 mm radius of curvature full-reflective mirror and a 25% reflective plane-parallel mirror as the output coupler. An intracavity thin film polarizer selected the wavelength and was tuned to transmission in Q-switch mode for the 1053 nm line. The laser diodes were powered by pump square pulses 150 µs long with a current of 100 A. The output energy was fixed at 67 mJ while the pulse duration was 19 ns.

After the oscillator, the first component to be installed was a Faraday isolator to protect the oscillator from the feedback provided by reflections in subsequent stages. Without the Faraday isolator, despite the low emission cross-section of the 1053 nm line of Nd:YLF and the anti-reflection coating of the rods, feedback from the amplifiers would couple to the cavity of the oscillator and parasitic QCW lasing was observed in this setup.

A telescope located after the isolator collimated and increased the beam size to a diameter of 4.8 mm. The collimated beam then traverses the first pair of amplifiers. The two pumping heads were operating with 300 µs long pump pulses and 100 A. Up to 540 mJ per pulse was achieved for 67 mJ of input and single pass configuration, which results in total extracted energy of 473 mJ, 195 mJ from the first amplifier and 278 mJ from the second amplifier.

Due to the natural birefringence of Nd:YLF, thermal-induced depolarization is almost non-existent in the oscillator or any of the two pairs of amplifiers, measured as less than 4% at full power. The condition for low birefringence at this pair of amplifiers is that the input polarization is perfectly aligned to the actual optical axis; for fine tuning of the polarization a half waveplate is situated before each and every amplification stage.

Thermal lensing is not an issue in these amplifiers due to the choice of the active medium. The factor dn/dT for the 1053 nm polarization of Nd:YLF is much weaker than that of other Nd-doped crystals such as Nd:YAG. Additionally, the coefficient is negative, so a beam experiencing thermal lensing on Nd:YLF will diverge instead of focusing, therefore damage risk is much lower in a laser using this crystal. However, the different thermal behavior of the optical axes introduces astigmatism in the beam.

A first SHG crystal was positioned after the first pair of amplifiers. The crystal was a type II KTP (Crystal Laser, France), which worked at 25 °C. Thanks to advances in crystal growing technology, we did not observe any power degradation due to gray-tracking during the time the laser was working. At that temperature we used the same cooling circuit of water as the pumping heads. This simplified the electronic circuit but did not introduce any noticeable instability in the SHG conversion although the time required for *turn-on* stabilization increased.

After the first SHG stage, to improve the efficiency of the laser, the unconverted infrared laser is further amplified in another chain of two amplifiers. A telescope is placed to collimate the beam which then enters the second pair of pumping heads and its energy is boosted to 465 mJ, a level similar to the output of the first pair of amplifiers.

To improve the overall efficiency of the laser, the fundamental laser radiation that is not converted to the second harmonic in this SHG crystal is not dumped and instead is further amplified in another chain of two amplifiers. With this method higher energy per pulse can be achieved while maintaining the same optics size and fluence. No degradation of the wavefront or polarization was found for the fundamental wavelength beam. The recycled fundamental harmonic beam is then collimated in a telescoped before entering the second pair of pumping heads, which boost the energy again to 465 mJ, a level similar to the output of the first pair of amplifiers.

A second KTP crystal, on an identical mount and temperature conditions as the first one, converts to the second harmonic the amplified recycled infrared radiation. With this configuration, the laser has two second harmonic outputs. A dichroic mirror sends the second harmonic towards the crystal to pump while the unconverted energy is stopped with a beam dump. While the maximum efficiency was about 55% individually at each crystal, this method of post-amplification of the recycled fundamental harmonic beam allows for an overall SHG efficiency of this laser of almost 70%. The overall efficiency can be defined as the ratio of the total second harmonic radiation energy and the total output energy; this behavior is pictured in Fig. 3a, while in Fig. 3b the absolute value of the second harmonic energy per pulse is represented as a function of the input infrared radiation at each KTP.

The final parameters of this MOPA laser are 500 mJ of energy per pulse at 527 nm wavelength divided in two beams of 250 mJ each and 19 ns pulse duration working at 100 Hz. The output energy of this laser was limited due to the size of the Nd:YLF rods. The duration of the pump pulses was limited to 300 µs, although more energy can be stored in the active medium if the pump pulses are extended to 500 µs. Our simulations predict that an energy per pulse and beam of 500 mJ at 527 nm can be obtained with an efficiency of 58% in the KTP.

4 Management of the thermal load

The management of the thermal lensing effect is of capital importance in the development of a high average power lasers, since it can lead to deformations of the spatial properties of the beam and optical damage in any element of the amplifiers.

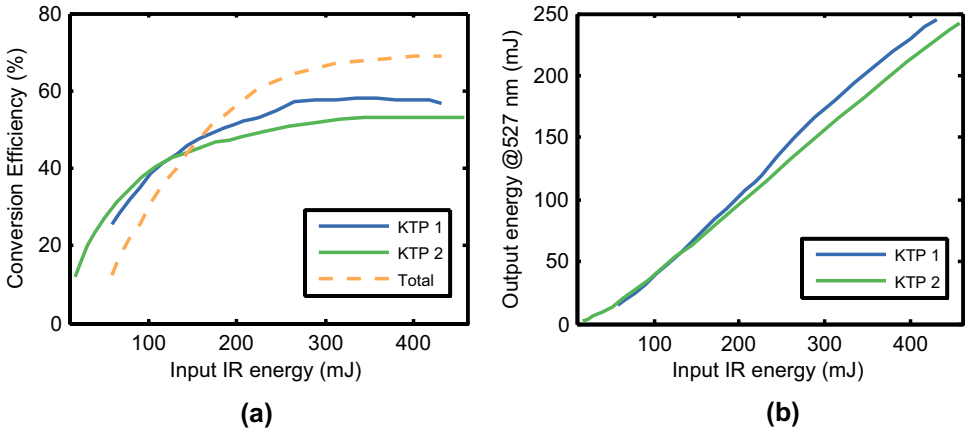

Fig. 3 **a** Plot of the efficiency of the second harmonic generation in the Nd:YLF MOPA. **b** Output energy @527 nm as a function of the input energy for both KTP crystals

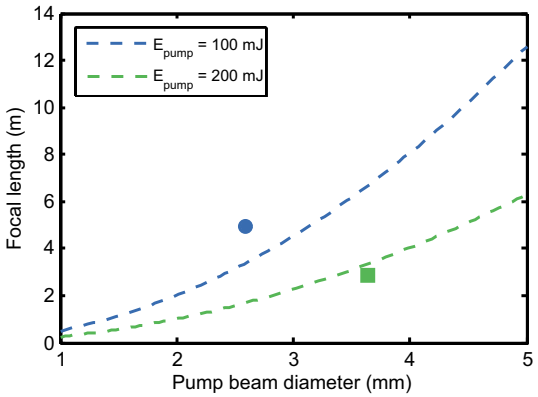

Fig. 4 Thermal lensing of the Ti:Sa crystal at the first multipass amplifier. The dashed lines represent calculations of the focal length using an analytical formula [14] both for 100 mJ and 200 mJ of pump power. The single dots represent experimental measurements of the thermal lensing focal length

In the Ti:Sa CPA laser, thermal lensing begins to be problematic at the first multipass stage, since the active medium is pumped by a maximum of 20 W of optical power, of which about 8 W are converted to heat. The focal length of this crystal was found to be 5000 mm when pumped with a fluence of 2 J/cm^2 using 100 mJ pump pulses or 2000 mm when using 200 mJ pulses, as can be seen in Fig. 4. The measurement of the optical power of the thermal lensing effect was carried out using a collimated He–Ne auxiliary laser beam and a CCD camera for measuring the beam size for several positions around the beam waist. This effect, if unchecked, can lead to poor beam quality and damage in any of the optics or the active medium, as the beam passes up to four times through this crystal. To compensate the action of thermal lensing in this amplifier and improve the extraction efficiency, we implemented a telescope situated prior to the first pass. The beam coming from the regenerative amplifier passes through a Galilean telescope where the distance between the positive and negative lens is chosen so that the beam exits with a size of 1.5 mm in diameter. This telescope does not collimate the beam but introduces some divergence so that the beam increases in size through amplification, compensating the heat-induced convergence and alleviating thermal lensing. However, the magnitude of the thermal lensing effect is moderately strong in the case of 200 mJ pump energy, therefore at least a convex-curved mirror has to be placed in the second pass to help the beam retain some divergence and grow for the last pass through the amplifier.

The development of the second multipass amplifier had to overcome more severe issues introduced by thermal lensing. In this stage, the total power pumped into the Ti:Sa crystal can reach 100 W and about 31% of this quantity is converted to heat that must be dissipated from the crystal. The pump beams were enlarged to a size of 8.5 mm of diameter at the position of the crystal, which is a fluence below 2 J/cm^2 for 1 J of energy. The Ti:Sa crystal was enclosed in a small vacuum chamber to decrease the cooling temperature to −20 °C using a mixture of water and ethylene glycol as the cooling fluid. The focal length when the crystal was pumped at full power was measured using the same method as for the first multipass, resulting in 2100 mm at a cooling temperature of −20 °C and 1500 mm at 15 °C.

To mitigate the action of thermal lensing throughout this multipass amplifier, we used a system of two telescopes situated between both amplifiers to introduce divergence in the seed beam, an approach similar to what has been proposed in other publications [15]. The input beam from the previous amplifier was enlarged to 5 mm of diameter using a telescope made of two curved mirrors. Afterwards, a Galilean telescope of low magnification was used to introduce divergence by changing the distance between the lenses. Due to the magnitude of thermal lensing effect, it was difficult to find a setup such that the divergence was enough to compensate for the thermal lensing accumulated through three passes. Instead, the idea is that the divergence introduced by the last telescope is enough to compensate for the thermal lensing of the first pass, then add a convex mirror between

the second and third passes. This spherical convex mirror has an incidence angle of 45°, which introduces a little astigmatism that can compensate the astigmatic behavior of the thermal lensing effect in this crystal due the spatial profile and overlap of the pump beams. A simple calculation shows that the distance δ between the lenses of the telescope has to be

$$\delta = \frac{f_2^2}{f_2 + f_T - L}, \tag{1}$$

where f_2 is the focal length of the positive lens, f_T is the focal length of the Ti:Sa crystal and L is the distance between the telescope and the active medium. Then, to compensate the thermal lensing of the additional passes, a convex mirror of radius of curvature −2000 mm was inserted after the second pass, to increase the divergence of the laser and to prevent the beam from leaving the amplifier converging.

5 Laser performance

The 5 nJ, large bandwidth pulses generated by the oscillator are stretched to an estimated duration of 100 ps in the stretcher. The energy is boosted in three amplification stages as described in Sect. 2.

The first amplification stage, the regenerative amplifier, produces 1.5 mJ per pulse for a total gain of 10^6 when pumped with 7 mJ after a total of 20 round trips through the resonator. One of the advantages of the regenerative amplifier is that the beam profile is naturally filtered by the resonator resulting in a Gaussian output profile (Fig. 5a). It has a diameter of 1.5 mm at the position of the telescope which magnifies the beam for the next amplifier.

However, a disadvantage of the regenerative amplifier is that the thin-film polarizer used to couple and uncouple the pulses out of the resonator generates pulse replicas separated in time by the time it would take the light to make a round trip, due to the reflectivity of the thin film polarizer. These pulse replicas turn into pre-pulses that decrease severely the contrast of the laser. To compensate for this effect, a saturable absorber is placed before the next amplification stage.

The next amplification stage is a multipass amplifier. It is pumped with 200 mJ from a doubled Nd:YLF laser. A total of 40 mJ per pulse is the output energy when the laser passes four times through the active medium and 30 mJ when the laser makes three passes. The output beam retains its Gaussian profile throughout this amplification stage as pictured in Fig. 5b. Another saturable absorber is placed at the exit of this amplifier to decrease further the intensity of the pre-pulses introduced at the regenerative amplifier; the transmission of the saturable absorber is 66%, therefore the energy drops to 26 mJ.

The last amplification stage is a multipass amplifier pumped by 1000 mJ originating from two identical Nd:YLF MOPAs as described in Sect. 3. The performance of the amplifier can be consulted in Fig. 6. It reaches a maximum

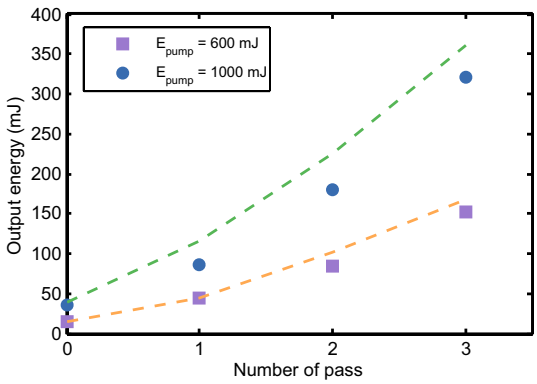

Fig. 6 Performance per pass of the second multipass amplifier when pumped with an energy of 600 mJ (purple squares) and 1000 mJ (blue circles). The dashed lines represent Frantz–Nodvik simulations

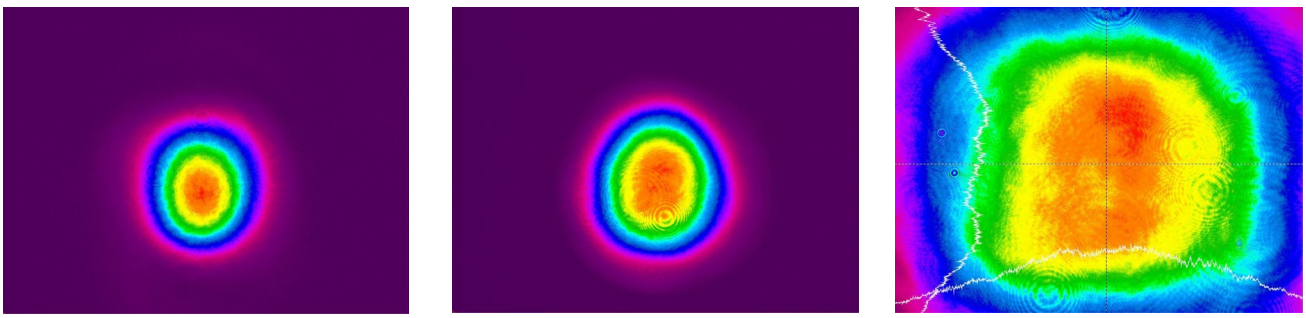

Fig. 5 Spatial profile of the laser beam (full energy) after each amplification stage: **a** regenerative amplifier, **b** first multipass amplifier and **c** second multipass amplifier

energy of 315 mJ per pulse in three passes, an amplification efficiency close to 30% which compares well with other reported similar laser systems and a Frantz–Nodvik model of amplification. The beam profile after three passes through the amplifier is pictured in Fig. 5c. It has lost symmetry and its gaussian shape resulting in a beam that resembles the multimode profile of the pump beams. The high fluence, thermal lensing and saturation of the amplification process are the main contributors to this change in beam profile. Although the beam is more intense in the center it has no hot-spots and the laser operated with high pointing stability, 24 µrad.

The spectral bandwidth of the laser also suffers modification through the amplification process due to gain narrowing and gain shifting, as shown in Fig. 7. The laser exits the regenerative amplifier with a FWHM bandwidth of about 27 nm but after the second multipass amplifier it has been reduced to 19 nm. The saturable absorber also contributes to narrowing, as it absorbs a portion of the spectrum due to chirping.

6 Compression and focusing

The size of the output beam coming from the second multipass amplifier is increased to 50 mm diameter as it goes through a collimating telescope before entering the compressor, which is located inside a vacuum chamber. The compressor features a Treacy design [16] comprising two diffraction gratings and a roof mirror. Both gratings are identical in characteristics to the one in the stretcher (1200 grooves/mm). The first order diffraction efficiency of each grating is higher than 90% and the overall efficiency of the compressor is 65.5%. Therefore, after compression the energy per pulse is reduced to 205 mJ. No thermal-induced effects were observed on the gratings during operation.

The pulse duration was measured with a Wizzler (Fastlite), which uses the technique of self-referenced spectral interferometry [17]. A feedback loop can be set up between this device and the spectral shaper Dazzler located after the stretcher to optimize the spectral shape to minimize dispersion, especially the third order term, which was found to be one which contributed the most to aberrations in the spectral phase. The pulse duration was determined to be 55 fs while the spectral bandwidth retrieved is 17 nm FWHM, close to the 52 fs of the transform limited pulse as seen in Fig. 8.

After the compressor, the laser beam enters the interaction chamber, where the laser is focused and the experiments are performed. The beam is focused through an off-axis parabola with a focal length of 100 mm and angle of 60°. The size of the focus was measured with a CCD camera

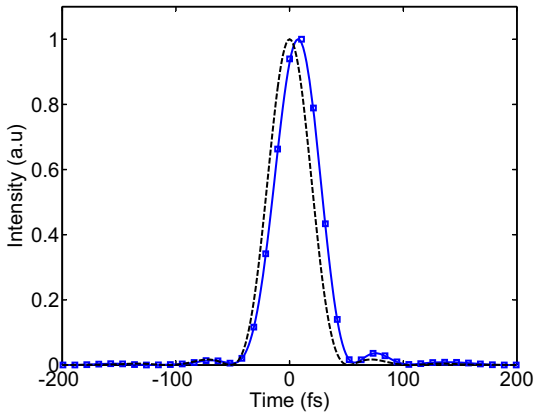

Fig. 8 Measured pulse duration. The dashed curve is the Fourier transform limited pulse. The solid curve represents the pulse duration corresponding to 55 fs FWHM

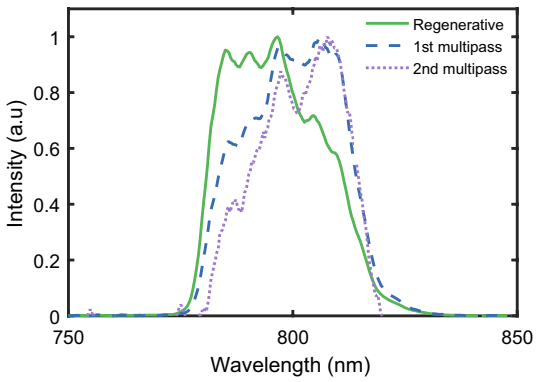

Fig. 7 Evolution of the normalized laser spectrum through the amplification stages. The straight line represents the spectrum after the regenerative amplifier, the dashed line after the first multipass and the pointed line after the second multipass amplifier

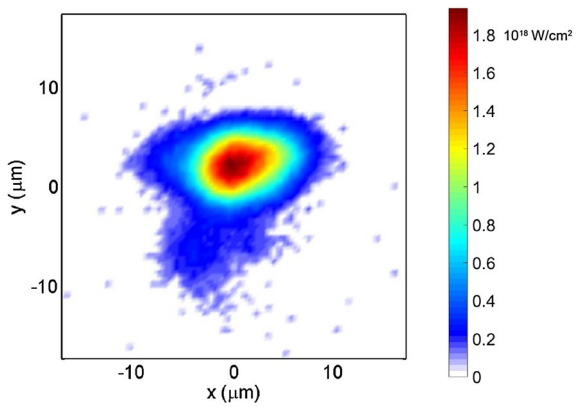

Fig. 9 Image captured a CCD camera of the focal spot of the Ti:Sa laser when focused with a 100-mm focal length off-axis parabola

and an aspheric lens for magnification, and it can be seen in Fig. 9. The spot size is $5 \times 9\,\mu m$ FWHM and the peak intensity is higher than $1.8 \times 10^{18}\,W/cm^2$. The percentage of the total energy enclosed in the area of the focal spot exceeds 82%. The lack of symmetry in the focal spot is likely caused by the use of spherical mirrors for the compensation of thermal lensing.

The contrast of the laser was measured using a fast photodiode, which provides valuable information especially about the ASE pedestal [18]. When the saturable absorbers were not installed in the setup, the contrast was 10^3 while it increased to 10^6 when they were present in the laser, which guarantees that the intensity of the prepulses is not high enough to create plasma. While the saturable absorbers were useful for the improvement of contrast, they had the drawback of absorbing part of the spectrum. As a result, the pulse duration increased from 45 to 55 fs.

This laser has been used in single-shot proton acceleration experiments were a maximum energy of 2 MeV has been reported using several thin-foil targets of different thickness and materials [19].

7 Conclusion

In conclusion, we have developed a reliable 3.8 TW peak power 100 Hz CPA Ti:Sa laser. The management of the high thermal load at the active media of the three amplification stages without cryogenic cooling was possible thanks to the implementation of passive optics as a means of alleviating thermal lensing. Although the wavefront suffered from heat-induced effects the laser could reach very high peak intensities when focused with an off-axis parabola without the need for adaptive optics. The pump lasers were diode-pumped solid state lasers especially designed for high average power operation, which is the main characteristic that differentiates this system from others. Remarkably, Nd:YLF performed better than Nd:YAG, both in high average power operation, particularly heat management, and energy per pulse output. This laser was developed to be used in high repetition rate plasma physics experiments, where the contrast of the laser is an important characteristic, and thus the need to include two saturable absorbers in the setup.

Future improvements will be directed towards the improvement of intensity, whether by reducing the pulse duration or increasing the energy of the laser. It is estimated that the pulse duration can be reduced to 30 fs after inserting an etalon filter, where the gain narrowing effect is strong while the energy of the laser can be increased with more powerful pump lasers. In recent experiments, a single Nd:YLF MOPA achieved 900 mJ at the wavelength of 527 nm, nearly doubling the current pump output.

Funding Centro para el Desarrollo Tecnológico Industrial (CDTI, Spain) within the INNPRONTA program, Grant no. IPT-20111027.

References

1. P. Zeitoun, G. Faivre, S. Sebban, T. Mocek, A. Hallou, M. Fajardo, D. Aubert, P. Balcou, F. Burgy, D. Douillet, S. Kazamias, G. de Lachèze-Murel, T. Lefrou, S. le Pape, P. Mercère, H. Merdji, A.S. Morlens, J.P. Rousseau, C. Valentin, Nature **431**(7007), 426–429 (2004)
2. V. Malka, S. Fritzler, E. Lefebvre, M.-M. Aleonard, F. Burgy, J.-P. Chambaret, J.-F. Chemin, K. Krushelnick, G. Malka, S.P.D. Mangles, Z. Najmudin, M. Pittman, J.-P. Rousseau, J.-N. Scheurer, B. Walton, A.E. Dangor, Science **298**(5598), 1596–1600 (2002)
3. H. Daido, M. Nishiuchi, A.S. Pirozhkov, Rep. Progress Phys. **75**(5), 056401 (2012)
4. A. Macchi, M. Borghesi, M. Passoni, Rev. Mod. Phys. **85**, 751–793 (2013)
5. T. Tajima, J.M. Dawson, Phys. Rev. Lett. **43**, 267–270 (1979)
6. M. Noaman-ul Haq, H. Ahmed, T. Sokollik, L. Yu, Z. Liu, X. Yuan, F. Yuan, M. Mirzaie, X. Ge, L. Chen, J. Zhang, Phys. Rev. Accel. Beams **20**, 041301 (2017)
7. D. Strickland, G. Mourou, Opt. Commun. **53**(3), 219–221 (1985)
8. G. Cheriaux, B. Walker, L.F. Dimauro, P. Rousseau, F. Salin, J.P. Chambaret, Opt. Lett. **21**(6), 414–416 (1996)
9. P. Tournois, Opt. Commun. **140**(4), 245–249 (1997)
10. R. Soulard, A. Brignon, S. Raby, E. Durand, R. Moncorgé, Appl. Phys. B **106**(2), 295–300 (2012)
11. J. Liu, L. Ge, L. Feng, H. Jiang, H. Su, T. Zhou, J. Wang, Q. Gao, J. Li, Chin. Opt. Lett. **14**(5), 051404 (2016)
12. A. Maleki, M.K. Tehrani, H. Saghafifar, M.H.M. Dindarlu, H. Ebadian, Laser Phys. **26**(2), 025003 (2016)
13. R. Lera, F. Valle-Brozas, S. Torres-Peiró, A.R. de-la Cruz, M. Galán, P. Bellido, M. Seimetz, J.M. Benlloch, L. Roso, Appl. Opt. **55**(33), 9573–9576 (2016)
14. R. Lausten, P. Balling, J. Opt. Soc. Am. B **20**(7), 1479–1485 (2003)
15. I. Nam, M. Kim, T.H. Lee, S.W. Lee, H. Suk, Curr. Appl. Phys. **15**(4), 468–472 (2015)
16. E. Treacy, IEEE J. Quantum Electron. **5**(9), 454–458 (1969)
17. A. Trisorio, S. Grabielle, M. Divall, N. Forget, C.P. Hauri, Opt. Lett. **37**(14), 2892–2894 (2012)
18. Y.-H. Cha, Y.-W. Lee, S.M. Nam, J.M. Han, Y.J. Rhee, B.D. Yoo, B.C. Lee, Y.U. Jeong, Appl. Opt. **46**(28), 6854–6858 (2007)
19. P. Bellido, R. Lera, M. Seimetz, A.R. de la Cruz, S. Torres-Peiró, M. Galán, P. Mur, I. Sánchez, R. Zaffino, L. Vidal, A. Soriano, S. Sánchez, F. Sánchez, M. Rodríguez-Álvarez, J. Rigla, L. Moliner, A. Iborra, L. Hernández, D. Grau-Ruiz, A. González, J. García-Garrigos, E. Díaz-Caballero, P. Conde, A. Aguilar, L. Roso, J. Benlloch, J. Instrum. **12**(05), T05001 (2017)